PCCP

PAPER

View Article Online
View Journal | View Issue

Open Access Article. Published on 20 November 2013. Downloaded on 10/16/2025 12:40:07 PM.
This article is licensed under a Creative Commons Attribution 3.0 Unported Licence.

Cite this: *Phys. Chem. Chem. Phys.*, 2014, **16**, 1139

Kinetics of CH_2OO reactions with SO_2, NO_2, NO, H_2O and CH_3CHO as a function of pressure†

Daniel Stone,[a] Mark Blitz,*[ab] Laura Daubney,[a] Neil U. M. Howes[a] and Paul Seakins[ab]

Received 16th October 2013,
Accepted 19th November 2013

DOI: 10.1039/c3cp54391a

www.rsc.org/pccp

Kinetics of CH_2OO Criegee intermediate reactions with SO_2, NO_2, NO, H_2O and CH_3CHO and CH_2I radical reactions with NO_2 are reported as a function of pressure at 295 K. Measurements were made under pseudo-first-order conditions using flash photolysis of CH_2I_2–O_2–N_2 gas mixtures in the presence of excess co-reagent combined with monitoring of HCHO reaction products by laser-induced fluorescence (LIF) spectroscopy and, for the reaction with SO_2, direct detection of CH_2OO by photoionisation mass spectrometry (PIMS). Rate coefficients for $CH_2OO + SO_2$ and $CH_2OO + NO_2$ are independent of pressure in the ranges studied and are $(3.42 \pm 0.42) \times 10^{-11}$ cm^3 s^{-1} (measured between 1.5 and 450 Torr) and $(1.5 \pm 0.5) \times 10^{-12}$ cm^3 s^{-1} (measured between 25 and 300 Torr), respectively. The rate coefficient for $CH_2OO + CH_3CHO$ is pressure dependent, with the yield of HCHO decreasing with increasing pressure. Upper limits of 2×10^{-13} cm^3 s^{-1} and 9×10^{-17} cm^3 s^{-1} are placed on the rate coefficients for CH_2OO + NO and $CH_2OO + H_2O$, respectively. The upper limit for the rate coefficient for $CH_2OO + H_2O$ is significantly lower than has been reported previously, with consequences for modelling of atmospheric impacts of CH_2OO chemistry.

1. Introduction

Criegee intermediates, carbonyl oxide biradicals with the general formula CR_2OO, are principally produced in the atmosphere following ozonolysis of unsaturated volatile organic compounds (VOCs) and are key species in the tropospheric oxidation of both biogenic and anthropogenic compounds.[1,2] The exothermicity of ozonolysis reactions leads to production of vibrationally excited Criegee intermediates with sufficient energy to undergo unimolecular decomposition to products including OH and HO_2,[3–6] representing a significant source of these key oxidising species in certain important environments.[7–9] However, collisional quenching of the nascent excited Criegee intermediate by N_2 or O_2, to produce stabilised Criegee intermediates, is competitive with the unimolecular decomposition processes at ambient pressures,[1,5] and reactions of stabilised Criegee intermediates have the potential to impact atmospheric budgets of NO_x (NO_x = NO + NO_2), NO_3, O_3, HO_x (HO_x = OH + HO_2), SO_2, H_2SO_4, sulfate aerosol and secondary organic aerosol (SOA).[5,10–17]

Despite their potential importance in atmospheric chemistry, and thus in the assessment and prediction of issues such as air quality and climate change, direct observations of Criegee intermediates have only recently been achieved.[10–12,18–20] Kinetics and product yields of Criegee intermediate reactions currently used in atmospheric models are subject to large uncertainties, owing to the reliance of previous investigations on indirect techniques involving measurements of stable species in complex ozonolysis experiments, in which there are several potential sources and sinks of the measured species.[1,2] Welz *et al.*[10] reported the first direct measurements of Criegee intermediate kinetics, where the photolysis of CH_2I_2 in the presence of O_2 was used to generate the CH_2OO Criegee intermediate at low pressure (4 Torr) and, using synchrotron photoionisation mass spectrometry (PIMS) at the Advanced Light Source (ALS), demonstrated unequivocally that the Criegee intermediate, CH_2OO, was being monitored:

$$CH_2I_2 + h\nu \rightarrow CH_2I + I \quad \text{(R1)}$$

$$CH_2I + O_2 \rightarrow CH_2OO + I \quad \text{(R2a)}$$

While reactions of CH_2OO with NO and water vapour were reported to be slow, the reactions of CH_2OO with SO_2 and NO_2 were shown to be significantly faster than indicated by the indirect methods. Rate coefficients for both $CH_2OO + SO_2$ and $CH_2OO + NO_2$, measured at a pressure of 4 Torr and temperature of 298 K, were both approximately 1000 times greater than previously assigned, implying a more significant role of Criegee intermediate chemistry in the atmosphere than expected.

The ability to produce CH_2OO following photolysis of CH_2I_2 in the presence of O_2[10] has also facilitated spectroscopic investigations of CH_2OO in the infrared[19] and ultraviolet,[20] and has been used to demonstrate the production of NO_3 in the reaction of CH_2OO with NO_2.[21] Subsequent work at the ALS has

[a] School of Chemistry, University of Leeds, Leeds, UK. E-mail: m.blitz@leeds.ac.uk
[b] National Centre for Atmospheric Science, University of Leeds, Leeds, UK

† Electronic supplementary information (ESI) available. See DOI: 10.1039/c3cp54391a

Open Access Article. Published on 20 November 2013. Downloaded on 10/16/2025 12:40:07 PM.
This article is licensed under a Creative Commons Attribution 3.0 Unported Licence.

investigated the reactions of CH_2OO with acetone, acetaldehyde and hexafluoroacetone at low pressures,[11] with theoretical investigation[22] of the reaction between CH_2OO and acetaldehyde (CH_3CHO) indicating pressure dependence of the reaction and collisional stabilisation of nascent reaction adducts to produce secondary ozonides (SOZs) at higher pressures which subsequently decompose to generate organic acids.

Taatjes *et al.*[12] have also recently demonstrated production of the CH_3CHOO Criegee intermediate following photolysis of CH_3CHI_2 in the presence of O_2. The structure of the CH_3CHOO Criegee intermediate gives rise to the possibility of *syn*- and *anti*-conformers, with the conformers sufficiently different in energy, and with a barrier to conversion, leading to the potential for their behaviour as distinct species. Using the synchrotron PIMS technique, Taatjes *et al.*[12] were not only able to identify both the *syn*- and *anti*-CH_3CHOO conformers, but were also able to assign separate rate coefficients for reactions of the two conformers with SO_2 and water vapour. The *anti*-conformer was shown to display greater reactivity towards both SO_2 and H_2O compared to the *syn*-conformer, with rate coefficients for reactions of both *syn*- and *anti*-conformers with SO_2 greater than previously expected.[12]

Field observations in a boreal forest in Finland have provided further evidence for rapid reactions between Criegee intermediates and SO_2, with measurements identifying the presence of oxidising species other than OH which are able to oxidise SO_2 to SO_3 and ultimately to produce H_2SO_4.[23] The presence of the unknown oxidising species was shown to be related to emissions of biogenic alkenes, and it was postulated that Criegee intermediates may be responsible, with laboratory measurements of H_2SO_4 production during alkene ozonolysis reactions in the presence of SO_2 and OH scavengers providing further support for the action of Criegee intermediates as atmospheric oxidants of SO_2.[23]

Implementation of increased Criegee intermediate + SO_2 reaction rates in atmospheric models has been shown to improve model simulations of H_2SO_4 in forested regions in Finland and Germany,[14] and global modelling has shown that while global production of H_2SO_4 increases by only 4%, there are increases of up to 100% in the boundary layer in tropical forests.[15] Further modelling work has shown that reactions of Criegee intermediates with SO_2 can compete with OH + SO_2 in a number of regions, and that Criegee + SO_2 reactions may be the dominant removal mechanism for SO_2 in certain areas and are major contributors to sulfate aerosol formation on a regional scale.[17] Air quality modelling over the U.S. displayed limited impacts of increased Criegee + SO_2 reaction rates on sulfate aerosol production in this region, but the impacts were shown to be highly dependent on the competition between Criegee + SO_2 and Criegee + H_2O, with a combination of increased Criegee + SO_2 and decreased Criegee + H_2O reaction rates leading to enhanced sulfate aerosol concentrations.[16] However, such studies have largely been based on the low pressure data for CH_2OO + SO_2 reported by Welz *et al.*[10] and there is considerable uncertainty regarding the upper limit for CH_2OO + H_2O.[2,17]

Theoretical work has provided support for rapid reactions between Criegee intermediates and SO_2,[13,24] with reactions proceeding *via* the initial barrierless formation of a cyclic secondary ozonide, and has enabled prediction of potential effects of pressure.[13] For CH_2OO + SO_2, it has been predicted that the reaction products at atmospheric pressure will be a mixture of HCHO + SO_3 (~68%), formyl sulfinic ester (HC(O)OS(O)OH) (~15%) and a singlet bisoxy diradical ($CH_2(O)O$) + SO_2 (~17%).[13] In contrast, reactions of larger Criegee intermediates, including CH_3CHOO, at ambient pressures are expected to result in production of stabilised secondary ozonide species, with little formation of SO_3, and therefore little impact on H_2SO_4 and sulfate aerosol.[13] Investigation of the reaction products and pressure dependence of Criegee intermediate reactions is thus essential to the accurate determination of their atmospheric impacts.

The yield of CH_2OO Criegee intermediates following CH_2I_2 photolysis in O_2 was studied by Huang *et al.*,[25] and in our previous work,[26] as a function of pressure. Both investigations indicate that the initial reaction between CH_2I radicals and O_2 (R2) produces a chemically activated species, $CH_2IO_2^{\#}$, which decomposes at low pressures to produce CH_2OO + I (R2a), but is collisionally stabilised at higher pressures to produce the CH_2IO_2 peroxy radical (R2b).

$$CH_2I_2 + h\nu \rightarrow CH_2I + I \quad \text{(R1)}$$

$$CH_2I + O_2 \rightarrow CH_2IO_2^{\#} \quad \text{(R2)}$$

$$CH_2IO_2^{\#} \rightarrow CH_2OO + I \quad \text{(R2a)}$$

$$CH_2IO_2^{\#} + M \rightarrow CH_2IO_2 + M \quad \text{(R2b)}$$

Our previous work[26] indicates a yield of ~18% CH_2OO following photolysis of CH_2I_2 in air at 760 Torr, with recent results from Huang *et al.*[27] in reasonable agreement. This result has potential significance for modelling of atmospheric chemistry in iodine-rich regions,[28–31] and also indicates potential for pressure dependent studies of CH_2OO kinetics using photolysis of CH_2I_2 in O_2.

In this work, we report kinetics of CH_2OO reactions with SO_2, NO_2, NO, H_2O and CH_3CHO at pressures between 25 and 450 Torr at a temperature of 295 K, using photolysis of CH_2I_2–O_2–N_2 mixtures under pseudo-first-order conditions combined with monitoring of the HCHO reaction products by laser-induced fluorescence (LIF) spectroscopy, and, for the CH_2OO + SO_2 reaction at ~1.5 Torr, direct monitoring of CH_2OO by photoionisation mass spectrometry (PIMS). We also report kinetics of the CH_2I + NO_2 reaction at pressures between 25 and 300 Torr at 295 K.

2. Experimental

2.1 Laser-induced fluorescence experiments

Apparatus and experimental procedures for the laser-induced fluorescence (LIF) experiments have been described elsewhere in detail,[26,32] therefore only a brief description is given here. Kinetics of CH_2OO reactions were studied by monitoring of HCHO reaction products by LIF spectroscopy. Radicals were generated by the laser flash photolysis of CH_2I_2–O_2–N_2 gas mixtures (R1 and R2) with the addition of excess co-reagent

 This journal is © the Owner Societies 2014

Open Access Article. Published on 20 November 2013. Downloaded on 10/16/2025 12:40:07 PM.
This article is licensed under a Creative Commons Attribution 3.0 Unported Licence.

(NO_2, NO, SO_2, H_2O or CH_3CHO) to ensure pseudo-first-order conditions. Experiments to investigate CH_2I + NO_2 kinetics were performed in the absence of O_2, while those to investigate CH_2OO + NO_2 were performed using a limited range of NO_2 concentrations in order to avoid production of HCHO through the reaction of CH_2I with NO_2 (see Section 3.1), whilst maintaining pseudo-first-order conditions.

CH_2I_2 (Sigma-Aldrich, 99%) was used as a dilute gas in N_2 either by filling a glass bulb containing liquid CH_2I_2 with N_2 or by bubbling a slow flow of N_2 through liquid CH_2I_2. Reagents (NO, NO_2, SO_2, CH_3CHO) were prepared at known concentrations in N_2 and stored in glass bulbs. NO (BOC Special Gases, 99.5%) was purified prior to use by a series of freeze–pump–thaw cycles. CH_2I_2, CH_3CHO (Sigma-Aldrich, 99.5%), NO_2 (Sigma-Aldrich, 99.5%), SO_2 (Sigma-Aldrich, 99.9%), N_2 (BOC, 99.99%) and O_2 (BOC, 99.999%) were used as supplied. Water vapour was added to the gas mixture by bubbling a known flow of N_2 gas through a bubbler containing deionised water at a known temperature. Gases were mixed in a gas manifold and passed into a six-way cross reaction cell at known flow rates (determined by calibrated mass flow controllers). The pressure in the reaction cell was monitored by a capacitance manometer (MKS Instruments, 626A) and controlled by throttling the exit valve to the reaction cell. The total gas flow rate through the reaction cell was adjusted with total pressure to maintain an approximately constant gas residence time in the cell ($\sim$0.1 s). All experiments were performed at T = (295 $\pm$ 2) K unless stated otherwise.

For experiments using NO_2, NO, CH_3CHO or H_2O as co-reagents, initiation of chemistry within the cell was achieved using an excimer laser (KrF, Tui ExciStar M) operating at λ = 248 nm with typical laser fluence in the range 30–80 mJ cm^{-2}. Experiments in which SO_2 was present as the co-reagent were performed at a photolysis wavelength of 355 nm (typical fluence $\sim$ 150 mJ cm^{-2}), generated by frequency tripling the output of a Nd:YAG laser (Spectron Laser Systems) to avoid potential multi-photon photolysis of SO_2 at shorter wavelengths.[33–35]

Production of HCHO was monitored by laser-induced fluorescence (LIF) of HCHO at λ $\sim$ 353.1 nm.[36] Approximately 2 to 4 mJ pulse^{-1} of laser light at $\sim$353.1 nm was generated by a dye laser (Lambda Physik, FL3002) operating on DMQ/dioxirane dye and pumped by a 308 nm excimer laser generating $\sim$50 mJ pulse^{-1} (XeCl, Lambda Physik LPX100). The output of the dye laser was passed through the reaction cell in an orthogonal axis to the 248 nm/355 nm photolysis laser output, with HCHO fluorescence detected in the visible region of the spectrum by a channel photomultiplier (CPM, Perkin-Elmer C1943P) orthogonal to both the photolysis laser and the LIF excitation laser beams. A Perspex filter was used to prevent scattered laser light from the photolysis laser and the LIF excitation laser reaching the CPM. The HCHO fluorescence signal was monitored as a function of time following photolysis of CH_2I_2 by varying the time delay between firing the photolysis laser and the LIF excitation laser through use of a delay generator (SRS DG535). Results from between 5 and 20 photolysis shots were typically averaged prior to analysis.

2.2 Photoionisation mass spectrometry experiments

Photoionisation mass spectrometry (PIMS) experiments were performed in this work to determine the kinetics of CH_2OO + SO_2 at low pressure ($\sim$1.5 Torr) and 295 K by direct monitoring of CH_2OO in reactions performed under pseudo-first-order conditions. The PIMS apparatus has been described previously in detail[32,37,38] and only a brief description is given here. Gas mixtures of CH_2I_2–O_2–N_2 and CH_2I_2–O_2–N_2–SO_2 were prepared in a gas handling line, with reagents and reagent preparation as described above for the LIF experiments, and introduced to the steel reaction flow tube (10.5 mm internal diameter, 70 cm in length) *via* calibrated mass flow controllers. The pressure in the reaction flow tube was monitored by a capacitance manometer (MKS Instruments, 626A) and controlled by throttling the exit valve to the flow tube.

Chemistry was initiated by a pulsed excimer laser (Lambda Physik, Compex 205) at a wavelength of 248 nm, with typical fluence of $\sim$50 mJ cm^{-2}, through reactions (R1) and (R2). A representative sample from the reaction mixture effused into a high vacuum chamber ($<10^{-5}$ Torr, maintained by diffusion and turbo pumps) *via* a 1 mm pinhole situated in the sidewall of the reaction flow tube. Components of the gas mixture were photoionised using 118 nm vacuum ultraviolet (VUV) laser light (typically 10^{11} photons pulse^{-1}), generated by frequency tripling of the third harmonic of a Nd:YAG laser (Continuum Powerlite, 8010) in a Xe gas cell, and passed across the effusing gas flow within 2–3 mm of the sampling pinhole. VUV light of 118 nm (equivalent to 10.5 eV) is sufficiently energetic to ionise CH_2OO (threshold = 10.02 eV), but is below the threshold required to ionise other isomers at m/z = 46 (dioxirane, threshold = 10.82 eV; formic acid, threshold = 11.33 eV).[10] Ions were sampled by the time of flight mass spectrometer (TOF-MS, Kore Technology Ltd), and detected by an electron multiplier. The ion signals were amplified and boxcar averaged on an oscilloscope and then stored on the control computer. The ion signals were monitored as a function of time following photolysis of CH_2I_2 by varying the time delay between the excimer laser and the Nd:YAG laser, used to generate the VUV radiation, through use of a delay generator (SRS DG35). These kinetic traces consisted of typically 200 time points, with typically between 10 and 25 shot averaging per time point.

3. Results and discussion

3.1 Photolysis of CH_2I_2–O_2–N_2 mixtures

Fig. 1 shows the HCHO fluorescence signal following photolysis of CH_2I_2–O_2–N_2 mixtures (*i.e.* in the absence of any additional co-reagent), resulting in production of HCHO through reactions (R1)–(R6):[26,32]

$$CH_2I_2 + h\nu \rightarrow CH_2I + I \quad \text{(R1)}$$

$$CH_2I + O_2 \rightarrow CH_2OO + I \quad \text{(R2a)}$$

$$CH_2I + O_2 + M \rightarrow CH_2IO_2 + M \quad \text{(R2b)}$$

$$CH_2OO + I \rightarrow HCHO + IO \quad \text{(R3)}$$

$$CH_2IO_2 + I \rightarrow CH_2IO + IO \quad \text{(R4)}$$

Open Access Article. Published on 20 November 2013. Downloaded on 10/16/2025 12:40:07 PM.
This article is licensed under a Creative Commons Attribution 3.0 Unported Licence.

$$CH_2IO_2 + CH_2IO_2 \rightarrow 2CH_2IO + O_2 \quad (R5)$$

$$CH_2IO \rightarrow HCHO + I \quad (R6)$$

Previous work in this laboratory[26] has shown that the yields of CH_2OO and CH_2IO_2 from (R2) are dependent on pressure, owing to initial formation of the excited species $CH_2IO_2^{\#}$, which can either decompose to produce the CH_2OO Criegee intermediate and iodine atoms (R2a) or can be collisionally stabilised to produce the peroxy radical CH_2IO_2 (R2b). Since subsequent reactions of both CH_2OO and CH_2IO_2 in the absence of any additional co-reagent result in production of HCHO, there is no change in the total HCHO yield as a function of pressure following photolysis of CH_2I_2–O_2–N_2 mixtures.

Production of HCHO in reactions (R1)–(R6) can be approximated by eqn (1):[26,32]

$$S_{HCHO,t} = S_0[\exp(-k_{loss}t)] + \frac{S_1 k_g'}{k_g' - k_{loss}}\left[\exp(-k_{loss}t) - \exp\left(-k_g' t\right)\right] \quad (1)$$

where $S_{HCHO,t}$ is the HCHO signal at time t, S_0 is the height of the HCHO signal at time zero, S_1 is the maximum HCHO signal, k_g' is the pseudo-first-order rate coefficient for HCHO growth, and k_{loss} is the rate coefficient representing the slow loss of HCHO from the detection region *via* diffusion. Although the HCHO growth through reactions (R1)–(R6) is not strictly first-order, our previous work[26] demonstrates that eqn (1) can faithfully reproduce the HCHO growth kinetics. In the presence of excess co-reagent (*e.g.* SO_2, NO_2) the kinetics of HCHO production from CH_2OO are under pseudo-first-order conditions. Fig. 1 shows the fits to HCHO production in the absence and presence of additional co-reagent, indicating the fidelity of the fit to the analytical equation.

In the absence of any additional co-reagent, the first-order rate coefficient approximating the production of HCHO, k_g', was found to vary from $\sim$300 s^{-1} to $\sim$3500 s^{-1}, depending on the concentration of CH_2I_2, and thus of I atoms, in the system,

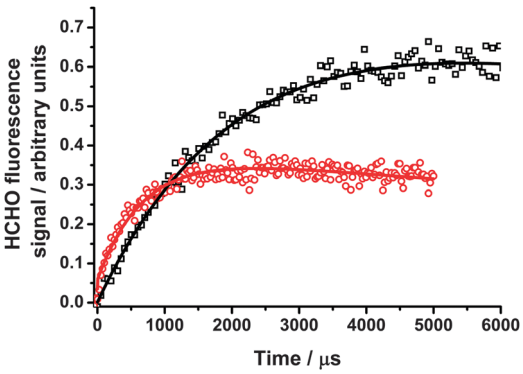

Fig. 1 HCHO fluorescence signals at 200 Torr following photolysis of CH_2I_2 in the presence of O_2 in the absence of any co-reagent (black open squares) and in the presence of NO_2 (red open circles). The fits to eqn (1) are shown by the solid lines, and give k_g' = (460 ± 30) s^{-1} in the absence of any additional co-reagent and k_g' = (1490 ± 50) s^{-1} in the presence of NO_2. The ratio of S_1 (eqn (1)) in the presence of NO_2 to that in the absence of NO_2 is 0.37.

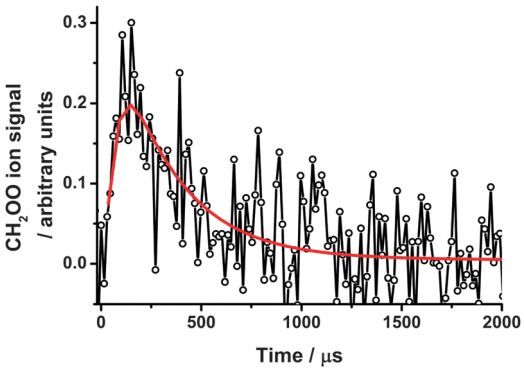

Fig. 2 CH_2OO ion signals at 1.5 Torr following photolysis of CH_2I_2–O_2–N_2 in the presence of SO_2, with the fit to eqn (2) (solid red line). For these data, k' = (3310 ± 450) s^{-1}.

in keeping with the work of Welz *et al.*[10] and Taatjes *et al.*[11] Some initial HCHO production was observed owing to multi-photon photolysis of CH_2I_2 and the subsequent rapid reaction of $^3CH_2$ with O_2, with S_0 typically no greater than 5–10% of S_1.[39–43]

3.2 $CH_2OO + SO_2$

The reaction of CH_2OO with SO_2 (R7) was investigated in separate experiments using the PIMS method to monitor CH_2OO and the LIF method to monitor HCHO production.

$$CH_2OO + SO_2 \rightarrow HCHO + SO_3 \quad (R7)$$

Experiments using the PIMS method were performed at a total pressure of 1.5 Torr. Fig. 2 shows a typical decay for CH_2OO observed in the presence of excess SO_2, with the pseudo-first-order rate coefficient for CH_2OO decay found by least-squares fitting to eqn (2):

$$S_{CH_2OO,t} = \frac{S_{max} k_{sampling}'}{k_{sampling} - k'}\left[\exp(-k't) - \exp\left(-k_{sampling}t\right)\right] \quad (2)$$

where $S_{CH_2OO,t}$ is the CH_2OO ion signal at time t, S_{max} is the maximum CH_2OO ion signal, k' is the pseudo-first-order rate coefficient for CH_2OO decay, and $k_{sampling}$ is the rate coefficient representing the transport of molecules in the reactor to the ionisation region ($\sim$30 000 s^{-1}, described in detail by Baeza-Romero *et al.*[38]).

The bimolecular rate coefficient for $CH_2OO + SO_2$ (k_7) determined using the PIMS method at 1.5 Torr was $(3.6 \pm 0.5) \times 10^{-11}$ cm^3 s^{-1} (Fig. 3), similar to the value of $(3.9 \pm 0.7) \times 10^{-11}$ cm^3 s^{-1} at 4 Torr reported by Welz *et al.*[10] and several orders of magnitude greater than the values typically used in atmospheric models.

The LIF experiments monitoring HCHO production from $CH_2OO + SO_2$ were performed over the pressure range 50–450 Torr, with SO_2 concentrations in the range 2.4×10^{14} to 1.6×10^{15} cm^{-3}. The HCHO growth (Fig. 4) was observed to display biexponential behaviour, with no decrease in the total HCHO yield compared to experiments performed in the absence of any co-reagent, indicating complete titration of both CH_2OO and

 This journal is © the Owner Societies 2014

Open Access Article. Published on 20 November 2013. Downloaded on 10/16/2025 12:40:07 PM.
This article is licensed under a Creative Commons Attribution 3.0 Unported Licence.

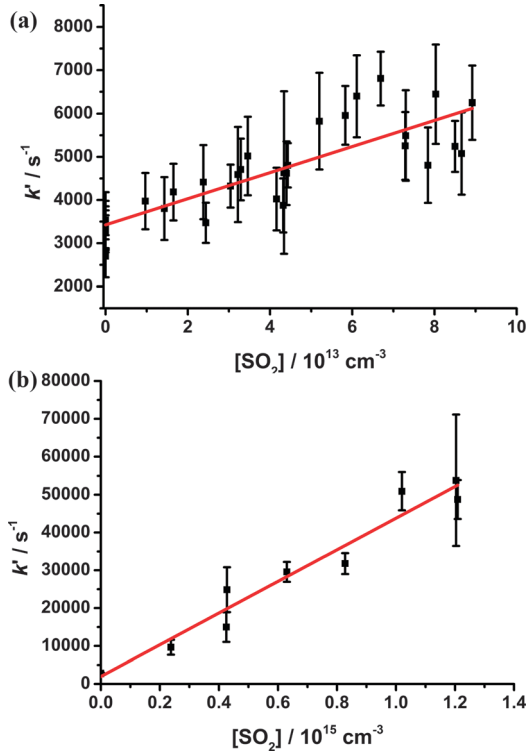

Fig. 3 (a) Pseudo-first-order rate coefficients (k') at 1.5 Torr, derived from fits to eqn (2), for the decay of the CH_2OO ion signal (m/z = 46, ionised using VUV radiation at 118 nm) following photolysis of CH_2I_2–O_2–N_2 in the presence of SO_2. Error bars are 1σ. The fit to the data (shown in red) gives the bimolecular rate coefficient for CHOO + SO_2 (k_7); (b) pseudo-first-order rate coefficients (k_{g1}') for the rapid HCHO production at 250 Torr following photolysis of CH_2I_2–O_2–N_2 in the presence of SO_2 derived from fits to eqn (3). Error bars are 1σ. The fit to the data (shown in red) gives the bimolecular rate coefficient for CHOO + SO_2 (k_7).

CH_2IO_2 to HCHO. Kinetic parameters were determined by fitting to eqn (3):

$$S_{\mathrm{HCHO},t} = S_0[\exp(-k_{\mathrm{loss}}t)] + \frac{S_1 f k_{g1}'}{k_{g1}' - k_{\mathrm{loss}}}\left[\exp(-k_{\mathrm{loss}}t) - \exp\left(-k_{g1}'t\right)\right] + \frac{S_1(1-f)k_{g2}'}{k_{g2}' - k_{\mathrm{loss}}}\left[\exp(-k_{\mathrm{loss}}t) - \exp\left(-k_{g2}'t\right)\right] \quad (3)$$

where $S_{\mathrm{HCHO},t}$ is the HCHO signal at time t, S_0 is the height of the HCHO signal at time zero, S_1 is the maximum HCHO signal, k_{g1}' is the pseudo-first-order rate coefficient for the fast HCHO growth, k_{g2}' is the pseudo-first-order rate coefficient for the slower HCHO growth, f is the fractional contribution of the fast growth process to the total HCHO yield (hence $(1-f)$ is the fractional contribution of the slower growth process to the total HCHO yield), and k_{loss} is the rate coefficient representing the slow loss of HCHO from the detection region *via* diffusion. For the SO_2 experiments (conducted using a photolysis wavelength of 355 nm) there was no contribution from S_0 (*i.e.* $S_0 = 0$).

The initial fast growth of HCHO displayed a linear dependence on [SO_2], while the slower growth was independent of

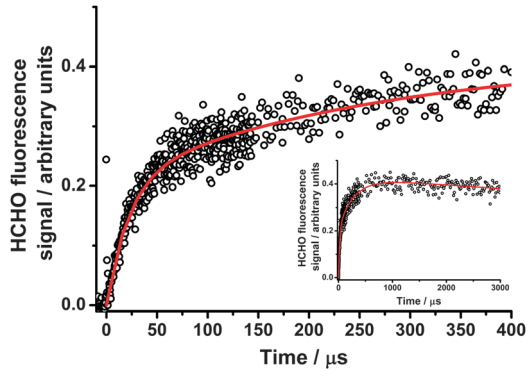

Fig. 4 HCHO fluorescence signals at 250 Torr following photolysis of CH_2I_2–O_2–N_2 in the presence of SO_2, with the fit to eqn (3) (solid red lines). The inset panel shows the evolution of the signal to longer times. For these data, k_{g1}' = (45 500 ± 2240) s^{-1}; k_{g2}' = (3580 ± 280) s^{-1}; k_{loss} = (40 ± 9) s^{-1}; f = (0.49 ± 0.01); S_1 = (0.43 ± 0.01).

[SO_2] and at a similar rate to the observed HCHO production in the absence of any additional co-reagent. The yields of HCHO from the faster growth process were consistent with production from CH_2OO + SO_2, while those from the slower process were consistent with production from reactions of CH_2IO_2 (*i.e.* reactions (R4)–(R6)). We thus determine k_7 from linear fits of k_{g1}' (eqn (3)) against [SO_2]. The validity of describing the system using eqn (3) is discussed in our previous work.[26]

Fig. 5 and Table 1 show the values of k_7 as a function of pressure. No significant dependence of k_7 on pressure was observed, with an average value of (3.42 ± 0.42) × 10^{-11} cm^3 s^{-1} for all experiments (PIMS and LIF) described in this work (all errors are 1σ unless stated otherwise). Moreover, there is no significant change in the HCHO yield from the reaction of CH_2OO with SO_2 as a function of pressure, indicating there is little stabilisation of reaction products. These results are consistent with the low pressure results obtained by Welz *et al.*[10] and theoretical work by Vereecken *et al.*,[13] and support arguments for an increased role of CH_2OO + SO_2 in the atmosphere.

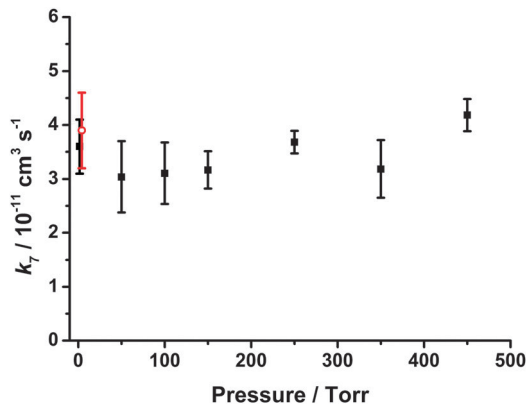

Fig. 5 Bimolecular rate coefficients for CH_2OO + SO_2 (k_7) as a function of pressure. Error bars are 1σ. The plot includes results from the PIMS experiments (at 1.5 Torr) and the LIF experiments (pressures ≥ 50 Torr). The data point shown by the red open circle is that determined by Welz *et al.*[10]

Open Access Article. Published on 20 November 2013. Downloaded on 10/16/2025 12:40:07 PM.
This article is licensed under a Creative Commons Attribution 3.0 Unported Licence.

Table 1 Bimolecular rate coefficients for $CH_2OO + SO_2$ (k_7) as a function of pressure. Errors are 1σ

Pressure (Torr)	k_7 (10^{-11} cm^3 s^{-1})	Ref.
1.5[a]	3.6 ± 0.5	This work
4	3.9 ± 0.7	Welz *et al.*[10]
50	3.04 ± 0.66	This work
100	3.11 ± 0.57	This work
150	3.17 ± 0.34	This work
250	3.68 ± 0.21	This work
350	3.19 ± 0.53	This work
450	4.18 ± 0.30	This work

[a] Data at 1.5 Torr are from the PIMS experiments.

Taatjes *et al.*[12] have also shown that the reaction of the C_2 Criegee intermediate, CH_3CHOO, with SO_2 at a pressure of 4 Torr is also significantly faster than previously expected, potentially indicating an increased role for $CH_3CHOO + SO_2$ in the atmosphere. However, theoretical calculations predict that reactions of larger Criegee intermediates will exhibit pressure dependence,[13] and that production of SO_3 in reactions of larger Criegee intermediates at atmospheric pressures is unlikely owing to stabilisation of SO_2–Criegee intermediate complexes to produce secondary ozonide species, thus reducing the impacts of SO_2 + Criegee intermediate reactions on H_2SO_4 and sulfate aerosol production.[13] Field observations and laboratory studies by Mauldin *et al.*[23] indicate that larger Criegee intermediates, such as those produced in the ozonolysis of monoterpenes, do impact on atmospheric concentrations of H_2SO_4 through oxidation of SO_2, but that the impacts may not be as great as those reported for CH_2OO, potentially owing to stabilisation of reaction products. Further work is thus required to investigate the effects of pressure on the reactions of larger Criegee intermediates. Moreover, modelled impacts of increases in the rates of Criegee intermediate reactions with SO_2 are highly dependent on the competition with rates of Criegee intermediate reactions with water vapour. We thus investigate $CH_2OO + H_2O$ in Section 3.6.

3.3 $CH_2I + NO_2$

Production of HCHO following photolysis of CH_2I_2–NO_2–N_2 mixtures was examined as a function of pressure to facilitate assessment of the competition between $CH_2I + O_2$ (R2) and $CH_2I + NO_2$ (R8) in $CH_2OO + NO_2$ experiments (Section 3.4).

$$CH_2I + NO_2 \rightarrow HCHO + \text{products} \quad (R8)$$

The production of HCHO could be described by eqn (1) (above), where $k_g' = k_8[NO_2]$, with concentrations of NO_2 between 1×10^{14} and 9×10^{14} cm^{-3}. Pseudo-first-order rate coefficients (k_g') were in the range ~5000 to 45 000 s^{-1}, and typically large compared to the rate coefficients describing HCHO production in the absence of any additional co-reagent (Section 3.1). The bimolecular rate coefficient k_8 was determined from plots of k_g' against $[NO_2]$ at each pressure (Fig. S1, ESI†), and was found to increase with increasing pressure (Fig. S2 and Table S1, ESI†), with a corresponding decrease in the HCHO yield as the pressure was increased (Fig. S3, ESI†).

A previous investigation of $CH_2I + NO_2$ at pressures of 2 to 5 Torr gave a value of $k_8 = (2.2 \pm 0.1) \times 10^{-11}$ cm^3 s^{-1}.[44] Results of this work show k_8 to be $(2.56 \pm 0.17) \times 10^{-11}$ cm^3 s^{-1} at 50 Torr, increasing to $(5.07 \pm 0.28) \times 10^{-11}$ cm^3 s^{-1} at 300 Torr.

The rate coefficient for reaction of CH_2I radicals with O_2 (R2), has been shown previously to be $\sim 1.6 \times 10^{-12}$ cm^3 s^{-1}.[45,46] Experiments to investigate HCHO production in the reaction of CH_2OO (produced by $CH_2I + O_2$) with NO_2 must therefore be conducted at sufficiently high $[O_2]$ to avoid complications owing to HCHO production from $CH_2I + NO_2$.

3.4 $CH_2OO + NO_2$

Experiments to investigate $CH_2OO + NO_2$ (R9) kinetics were performed with sufficient NO_2 concentrations (1.0×10^{14} to 1.4×10^{15} cm^{-3}) to ensure pseudo-first-order conditions for CH_2OO loss whilst also ensuring that $k_2[O_2] > k_8[NO_2]$ at all times to avoid potential complications owing to HCHO production through $CH_2I + NO_2$.

$$CH_2I_2 + h\nu \rightarrow CH_2I + I \quad (R1)$$

$$CH_2I + O_2 \rightarrow CH_2OO + I \quad (R2a)$$

$$CH_2I + NO_2 \rightarrow HCHO + \text{products} \quad (R8)$$

$$CH_2OO + NO_2 \rightarrow HCHO + NO_3 \quad (R9)$$

Fig. 1 shows the evolution of the HCHO signal following photolysis of CH_2I_2–O_2–N_2–NO_2 mixtures. Experiments in which NO_2 was used as a co-reagent resulted in a decrease in the total HCHO yield when compared to experiments performed in the absence of any co-reagent. We attribute this to the formation of the peroxy nitrate species $CH_2IO_2NO_2$ which inhibits formation of HCHO through reactions (R4)–(R6).

Experiments performed at 273 K to increase the lifetime of $CH_2IO_2NO_2$ with respect to dissociation to $CH_2IO_2NO_2$ did not result in any significant decrease in the HCHO yield compared to equivalent experiments at 295 K, indicating that the $CH_2IO_2NO_2$ lifetime at 295 K is sufficiently long to minimise production of HCHO from CH_2IO_2. Thus, while there is a small contribution to the HCHO signal owing to rapid chemistry following multi-photon photolysis of CH_2I_2, the growth of HCHO observed following photolysis of CH_2I_2–O_2–N_2–NO_2 mixtures can be attributed to $CH_2OO + NO_2$ (R9) exclusively.

The pseudo-first-order rate coefficient for the reaction of CH_2OO with NO_2 was determined by least-squares fitting to eqn (1), with $k_g' = k_9[NO_2]$. The bimolecular rate coefficient for $CH_2OO + NO_2$ (k_9) was subsequently determined from plots of k_g' against $[NO_2]$, as shown in Fig. 6. Fits to experimental data using the numerical integration package Kintecus[47] to determine k_9, detailed in the ESI,† gave results within 10% of those obtained using the analytical expression (eqn (1)).

Values for k_9 as a function of pressure are shown in Fig. 7 and Table 2. No significant dependence of k_9 on total pressure was observed over the pressure range investigated (25 to 300 Torr), with an average value of $k_9 = (1.5 \pm 0.5) \times 10^{-12}$ cm^3 s^{-1}. Errors in k_9 include the 1σ errors in the fits to the bimolecular plots at each pressure and an error of ±10% to account for any differences

Open Access Article. Published on 20 November 2013. Downloaded on 10/16/2025 12:40:07 PM.
This article is licensed under a Creative Commons Attribution 3.0 Unported Licence.

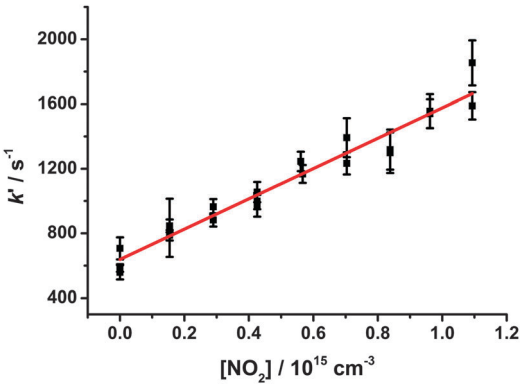

Fig. 6 Pseudo-first-order rate coefficients (k_9') for HCHO production at 50 Torr, derived from fits to eqn (1), following photolysis of CH_2I_2–O_2–N_2 in the presence of NO_2. Error bars are 1σ. The fit to the data (shown in red) gives the bimolecular rate coefficient for $CH_2OO + NO_2$ (k_9).

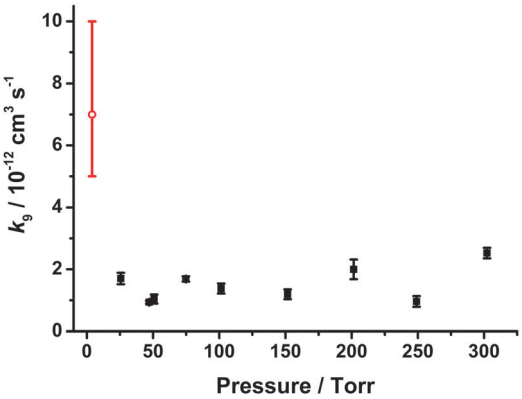

Fig. 7 Bimolecular rate coefficients for $CH_2OO + NO_2$ (k_9) as a function of pressure. Error bars are 1σ. The data point shown by the red open circle is that determined by Welz *et al.*[10]

Table 2 Bimolecular rate coefficients for $CH_2OO + NO_2$ (k_9) as a function of pressure. Errors include the 1σ in the fits to the bimolecular plots and an error of ±10% to account for any differences between the fits using the analytical expression and those obtained by numerical integration

Pressure (Torr)	k_9 (10^{-12} cm^3 s^{-1})	Ref.
4	7^{+3}_{-2}	Welz *et al.*[10]
25[a]	1.70 ± 0.38	This work
50[a]	1.04 ± 0.27	This work
50[b]	0.94 ± 0.16	This work
75[a]	1.69 ± 0.28	This work
100[a]	1.38 ± 0.33	This work
150[a]	1.19 ± 0.30	This work
200[a]	2.00 ± 0.56	This work
250[a]	0.96 ± 0.29	This work
300[a]	2.53 ± 0.47	This work

[a] Measured using N_2 as the bath gas. [b] Measured using O_2 as the bath gas.

between fits using the analytical expression and those obtained by numerical integration (see ESI†).

Yields of HCHO in the presence of NO_2, determined relative to experiments performed in the absence of NO_2 (*i.e.* production through reactions (R3)–(R6)), were consistent with the yields of CH_2OO determined in our previous work[26] (Fig. 8). This result demonstrates that ~100% of CH_2OO is titrated to HCHO by $CH_2OO + NO_2$, indicating a lack of pressure dependence in k_9, and that there is insignificant HCHO production from CH_2IO_2 in the presence of NO_2. Recent measurements by Ouyang *et al.*[21] have demonstrated the production of NO_3 at atmospheric pressure from the reaction of CH_2OO with NO_2, thus also suggesting little stabilisation of reaction products to a secondary ozonide species in this system.

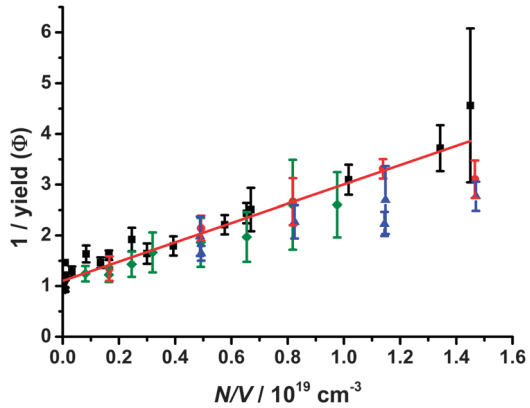

Fig. 8 Stern–Volmer plot showing (inverse) yields of CH_2OO as a function of pressure from the reaction of CH_2I with O_2. Results from our previous work are shown for experiments monitoring iodine atom production in the system (black squares), and monitoring of HCHO production in experiments with SO_2 (blue triangles) and NO (red circles), with the best fit line (red). Yields of HCHO from the reaction of CH_2OO with NO_2 (this work, green diamonds), determined relative to the HCHO yields in the absence of NO_2 (*i.e.* through reactions (R3)–(R6)), suggest that there is 100% titration of CH_2OO to HCHO in the presence of NO_2 at all pressures (*i.e.* there is no stabilisation of reaction products), and that there is little production of HCHO from CH_2IO_2 in the system. The fit to our previous work (comprising data from the I atom, NO and SO_2 experiments) gives an intercept of 1.10 ± 0.23 and a slope of (1.90 ± 0.22) × 10^{-19} cm^3. The NO_2 experiments give an intercept of 1.05 ± 0.12 and a slope of (1.70 ± 0.18) × 10^{-19} cm^3.

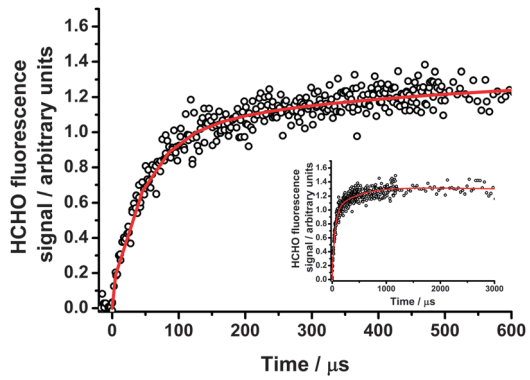

Fig. 9 HCHO fluorescence signals at 250 Torr following photolysis of CH_2I_2–O_2–N_2 in the presence of NO, with the fit to eqn (3) (solid red lines). The inset panel shows the evolution of the signal to longer times. For these data, k_{g1}' = (24 800 ± 1400) s^{-1}; k_{g2}' = (2660 ± 320) s^{-1}; k_{loss} = (10 ± 2) s^{-1}; f = (0.70 ± 0.02); S_1 = (1.33 ± 0.01).

Open Access Article. Published on 20 November 2013. Downloaded on 10/16/2025 12:40:07 PM.
This article is licensed under a Creative Commons Attribution 3.0 Unported Licence.

No significant difference in k_9 or in yields of HCHO were observed between experiments performed in O_2 bath gas and N_2 bath gas (results shown in Table 2), providing further evidence for similar quenching of the nascent excited $CH_2IO_2^{\#}$ species (produced in (R2)) by O_2 and N_2, as discussed in our previous work.[26]

Results for k_9 obtained in this work, while lower than those reported by Welz *et al.*,[10] are on the same order of magnitude, and demonstrate a significantly faster reaction between CH_2OO and NO_2 than suggested by previous indirect measurements.[1]

3.5 CH_2OO + NO

Production of HCHO following photolysis of CH_2I_2–O_2–N_2 mixtures in the presence of excess NO (3.6×10^{14} to 1.7×10^{15} cm^{-3}) exhibits biexponential growth, as shown in Fig. 9, similar to experiments with SO_2. Again, no decrease in the total HCHO yield compared to experiments performed in the absence of any co-reagent, indicating complete titration of both CH_2OO and CH_2IO_2 to HCHO. Kinetic parameters for the processes contributing to HCHO production were obtained by fitting to eqn (3) (above).

The rate coefficient describing the fast HCHO growth process, k_{g1}', was observed to increase linearly with increasing [NO], with the slope of a plot of k_{g1}' against [NO] giving a bimolecular rate coefficient of $(1.07 \pm 0.06) \times 10^{-11}$ cm^3 s^{-1} at 250 Torr (Fig. S4, ESI†). The rate coefficient describing the slower HCHO growth, k_{g2}', was found to be independent of [NO], and similar to the rate coefficient for HCHO production obtained in the absence of NO. Reactions of peroxy radicals (RO_2) with NO are well established, and are typically on the order of 10^{-12} to 10^{-11} cm^3 s^{-1},[48,49] with a rate coefficient for CH_3O_2 + NO of 7.2×10^{-12} cm^3 s^{-1},[49] while Welz *et al.*[10] reported an upper limit of 6×10^{-14} cm^3 s^{-1} for the rate coefficient for CH_2OO with NO. Thus, in contrast to the experiments with SO_2, we attribute the fast HCHO growth to the rapid decomposition of CH_2IO (R6), produced in the reaction of CH_2IO_2 with NO (R10) and assign $k_{10} = (1.07 \pm 0.06) \times 10^{-11}$ cm^3 s^{-1} at 250 Torr.

$$CH_2IO_2 + NO \rightarrow CH_2IO + NO_2 \qquad (R10)$$

$$CH_2IO \rightarrow HCHO + I \qquad (R6)$$

The slower HCHO growth thus contains contributions from CH_2OO + I (R3) and potentially CH_2OO + NO (R11). In the absence of NO, production of HCHO was observed with a pseudo-first-order rate coefficient of 1860 ± 100 s^{-1} (eqn (1)). On addition of up to 1.7×10^{15} cm^{-3} NO, the average value for the rate coefficient describing the slow HCHO growth (k_{g2}' in eqn (3)) was 1800 ± 340 s^{-1}. Any potential influence of NO on the observed rates of HCHO production is assumed to be within the error of the experiment, and we thus place an upper limit of 2×10^{-13} cm^3 s^{-1} on the rate coefficient for reaction of CH_2OO + NO (k_{11}).

$$CH_2OO + NO \rightarrow HCHO + NO_2 \qquad (R11)$$

The upper limit for k_{11} determined here is higher than that reported by Welz *et al.* ($k_{11} < 6 \times 10^{-14}$ cm^3 s^{-1}), owing to increased uncertainties associated with the biexponential fit, relatively low concentrations of NO, and higher concentrations of CH_2I_2 used in these experiments compared to those performed by Welz *et al.*, which lead to increased iodine atom concentrations in this work and thus increased rates of HCHO production through CH_2OO + I (R3). In subsequent experiments (notably those used to investigate the kinetics of CH_2OO + H_2O) lower CH_2I_2 concentrations were used by changing the delivery method for CH_2I_2. There are also additional uncertainties in the rate coefficients for reactions with NO owing to the potential for production of NO_2 in the gas lines leading to the reaction cell through oxidation of NO by O_2 (the gas mixture has a residence time of ~1 s in the gas lines leading from the mixing line to the reaction cell), leading to the potential for contributions to the observed HCHO growth from reactions involving NO_2.

3.6 CH_2OO + H_2O

Welz *et al.* did not observe any change in the rate of CH_2OO decay on addition of water vapour to the system, and reported an upper limit of 4×10^{-15} cm^3 s^{-1} for the rate coefficient for reaction of CH_2OO with H_2O (R12):

$$CH_2OO + H_2O \rightarrow HCHO + H_2O_2 \qquad (R12)$$

Similarly to the results of Welz *et al.*, the addition of water vapour to the LIF experiments in this work did not result in any significant change to the rate of HCHO production. The total HCHO yield was also unaffected by the presence of water vapour, indicating complete titration of CH_2OO and CH_2IO_2 to HCHO through reactions (R3)–(R6). Fig. 10 shows the HCHO fluorescence signals following photolysis of CH_2I_2–O_2–N_2 in the absence and presence of water vapour. While the HCHO signal is reduced in the presence of water vapour, there is no change in the kinetics and the reduction in signal is attributed to increased fluorescence quenching by water vapour.

At 200 Torr the pseudo-first-order rate coefficient for HCHO production was determined to be 41 ± 15 s^{-1} by fitting to eqn (1), and was lower than the typical values reported in Section 3.1 as a result of lower concentrations of CH_2I_2 to reduce the rate of

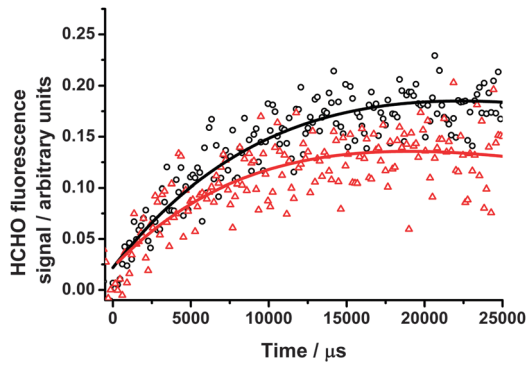

Fig. 10 HCHO fluorescence signals at 200 Torr following photolysis of CH_2I_2–O_2–N_2 in the absence (black open circles) and presence of water vapour (red open triangles), with the fits to eqn (1) (solid lines). The differences in the amplitude of the signal result from the quenching of the fluorescence signal by H_2O. For these data, k_g' = (41 ± 15) s^{-1} in the absence of water vapour and k_g' = (52 ± 13) s^{-1} in the presence of water vapour.

Open Access Article. Published on 20 November 2013. Downloaded on 10/16/2025 12:40:07 PM. This article is licensed under a Creative Commons Attribution 3.0 Unported Licence.

HCHO production through radical–radical reactions in the absence of water vapour. On addition of up to 1.7×10^{17} cm^{-3} water vapour to the system, a value of 52 ± 13 s^{-1} was obtained, with no obvious dependence on the concentration of water vapour added. Owing to the higher total pressures used in this work, enabling the addition of a higher number density of water vapour to the system compared to the low pressure experiments by Welz *et al.*, we are able to place an upper limit of 9×10^{-17} cm^3 s^{-1} on k_{12} at 295 K by assuming any influence of water vapour is within the error of the experiment. Ouyang *et al.*[21] have reported a value for k_{12} of $(2.5 \pm 1) \times 10^{-17}$ cm^3 s^{-1} at 760 Torr, determined in a relative rate experiment monitoring NO_3 production and using the absolute value for k_9 ($CH_2OO + NO_2$) reported by Welz *et al.*[10] (7×10^{-12} cm^3 s^{-1}). Using the relative rate coefficient ratio reported by Ouyang *et al.*, with the value for k_9 determined in this work (1.5×10^{-12} cm^3 s^{-1}), a value of $k_{12} = 5.4 \times 10^{-18}$ cm^3 s^{-1} can be obtained.

Modelling studies investigating the impacts of CH_2OO chemistry on the atmospheric oxidation of SO_2 may therefore be underestimating the effects of increasing the rate coefficient for $CH_2OO + SO_2$ owing to overestimation of the competition with $CH_2OO + H_2O$, resulting in more significant impacts on atmospheric production of H_2SO_4 and sulfate aerosol than indicated thus far. However, Taatjes *et al.*[12] have shown that the *anti*-CH_3CHOO Criegee intermediate does react with water vapour ($k = (1.0 \pm 0.4) \times 10^{-14}$ cm^3 s^{-1}), and the lack of reaction between CH_2OO and water vapour may not be representative of all Criegee intermediates. Modelling of Criegee chemistry in forested regions in Finland and Germany has indicated that concentration of the CH_2OO Criegee intermediate is only ~20–33% of the concentrations of larger Criegee intermediates derived from monoterpenes,[14] with global modelling indicating that the production rate of CH_2OO comprises ~40% of the total global production rate of all Criegee intermediates.[15] The chemistry of larger Criegee intermediates warrants further attention.

3.7 $CH_2OO + CH_3CHO$

The reactions of Criegee intermediates with carbonyl compounds are of interest not only for their potential atmospheric relevance, but also to facilitate the use of carbonyl compounds as scavengers of Criegee intermediates in alkene ozonolysis experiments, enabling the determination of product yields of ozonolysis reactions.

Horie *et al.*[50] studied the relative rates of CH_2OO reactions with CH_3CHO (R13) and CF_3COCF_3 (R14) at 730 Torr in synthetic air using FT-IR spectroscopy to monitor the decay of CF_3COCF_3 and the production of the secondary ozonide propene ozonide (methyl-1,2,4-trioxolane) from the reaction with CH_3CHO, and found the reaction with CF_3COCF_3 to be 13 times faster than that with CH_3CHO.

$$CH_2OO + CH_3CHO \rightarrow \text{products} \quad (R13)$$

$$CH_2OO + CF_3COCF_3 \rightarrow \text{products} \quad (R14)$$

Secondary ozonide products were observed by Horie *et al.* for both (R13) and (R14) at 730 Torr, while photoionisation mass spectrometry experiments by Taatjes *et al.*[11] at 4 Torr observed a secondary ozonide product for (R14) but not for (R13). Absolute rate coefficients for $CH_2OO + CH_3CHO$ and $CH_2OO + CF_3COCF_3$ were measured by Taatjes *et al.*[11] at 4 Torr in He by direct monitoring of CH_2OO, with results indicating the reaction with CF_3COCF_3 to be ~32 times faster than that with CH_3CHO and $k_{13} = (9.4 \pm 0.7) \times 10^{-13}$ cm^3 s^{-1} at 4 Torr. As discussed by Taatjes *et al.*,[11] the differences between the results of Horie *et al.* and Taatjes *et al.* may arise from differences in the fall-off behaviour of the two reactions, indicating pressure dependence of one or both of the reactions over the range of pressures investigated. Differences in product observations between the two studies also suggest pressure dependence in k_{13}. In the low pressure experiments, Taatjes *et al.* do not observe formation of secondary ozonide products. At 730 Torr, propene ozonide was observed as the major product of (R13), indicating collisional stabilisation of the nascent secondary ozonide at high pressures. Recent theoretical work[22] has investigated the potential energy surface for the reaction of CH_2OO with CH_3CHO, and supports the observed pressure dependence of the reaction. Reaction products are predicted to be collisionally stabilised to a secondary ozonide (SOZ) species, with significant production of the SOZ at atmospheric pressure (760 Torr) and the SOZ dominating the reaction products at pressures above 1000 Torr.

Pressure dependent kinetics are expected to be typical for reactions of larger Criegee intermediates with atmospherically relevant species, including SO_2, and investigation of the $CH_2OO + CH_3CHO$ system may therefore provide insight to the behaviour of other Criegee intermediates.

In this work, we investigate HCHO production from $CH_2OO + CH_3CHO$ (R13) at total pressures between 25 and 300 Torr and concentrations of CH_3CHO in the range 2×10^{14} to 1×10^{15} cm^{-3}. Production of HCHO displayed single exponential growth, and the HCHO fluorescence signal was fitted to eqn (1) (Fig. 11). Fig. 12 shows the bimolecular plot used to determine k_{13} at 25 Torr, giving $k_{13} = (1.48 \pm 0.04) \times 10^{-12}$ cm^3 s^{-1} at 25 Torr. The HCHO yield from (R13) (corrected for any HCHO production from CH_2IO_2 in reactions (R4)–(R6) using the results of our previous work) was observed to decrease with increasing pressure, indicating stabilisation of the $CH_2OO + CH_3CHO$ reaction product at higher pressures (R13b) and pressure dependence in k_{13}.

$$CH_2OO + CH_3CHO \rightarrow CH_2OO\text{–}CH_3CHO^{\#}$$

$$CH_2OO\text{–}CH_3CHO^{\#} \rightarrow HCHO + CH_3C(O)OH \quad (R13a)$$

$$CH_2OO\text{–}CH_3CHO^{\#} + M \rightarrow \text{propene ozonide} + M \quad (R13b)$$

Fig. 13 shows the Stern–Volmer plot for HCHO yields from (R13), giving an intercept of 1.19 ± 0.39 and slope (k_{13b}/k_{13a}) of $(1.09 \pm 0.08) \times 10^{-18}$ cm^3. Using an intercept of 1, at 4 Torr we estimate a yield of HCHO of 88%, with a yield of 4% at 730 Torr, reconciling the results of Taatjes *et al.*[11] and Horie *et al.*[50] and in agreement with theoretical work of Jalan *et al.*[22]

Owing to the decrease in HCHO yield with increasing pressure, assignment of the kinetics of (R13) at pressures above 25 Torr is challenging. Using the results of Taatjes *et al.*[11] at 4 Torr ($k_{13} = (9.5 \pm 0.7) \times 10^{-13}$ cm^3 s^{-1}), together with those

Open Access Article. Published on 20 November 2013. Downloaded on 10/16/2025 12:40:07 PM.
This article is licensed under a Creative Commons Attribution 3.0 Unported Licence.

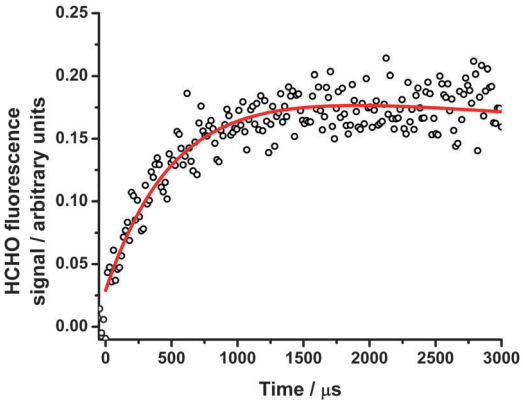

Fig. 11 HCHO fluorescence signals at 25 Torr following photolysis of CH_2I_2–O_2–N_2 in the presence of CH_3CHO, with the fit to eqn (1) (solid red line). For these data, k_g' = (2040 ± 120) s^{-1}.

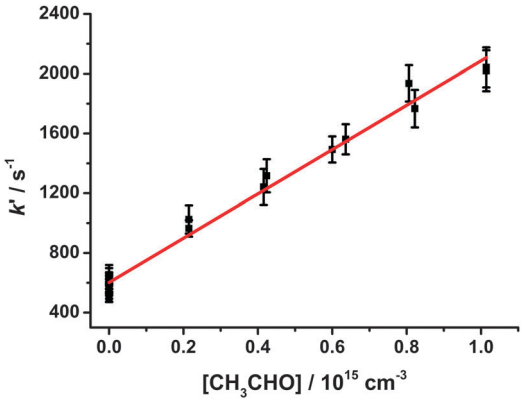

Fig. 12 Pseudo-first-order rate coefficients (k_g') for HCHO production at 25 Torr, derived from fits to eqn (1), following photolysis of CH_2I_2–O_2–N_2 in the presence of CH_3CHO. Error bars are 1σ. The fit to the data (shown in red) gives the bimolecular rate coefficient for CH_2OO + CH_3CHO (k_{13}).

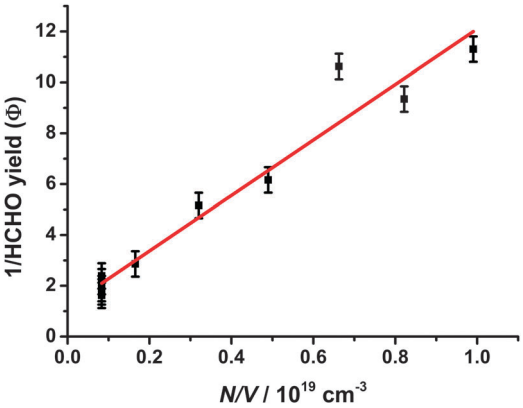

Fig. 13 Stern–Volmer analysis for HCHO yields from CH_2OO + CH_3CHO (R13) (corrected for HCHO production from CH_2IO_2 chemistry) as a function of total pressure, with the fit to the data (red). Error bars are 1σ.

determined here at 25 Torr (k_{13} = (1.48 ± 0.04) × 10^{-12} cm^3 s^{-1}), 50 Torr (~2.2 × 10^{-12} cm^3 s^{-1}) and the determination of k_{13b}/k_{13a} from the Stern–Volmer plot ((1.09 ± 0.08) × 10^{-18} cm^3), we estimate a low pressure limit ($k_{13,0}$) of ~1.6 × 10^{-29} cm^6 s^{-1} and a high pressure limit ($k_{13,\infty}$) of ~1.7 × 10^{-12} cm^3 s^{-1} (see ESI†).

4. Conclusions

Reactions of the CH_2OO Criegee intermediate with NO_2, NO, SO_2, H_2O and CH_3CHO have been investigated over a range of pressures. The reactions of CH_2OO with NO_2, SO_2 and CH_3CHO are rapid, in agreement with recent measurements by Welz *et al.*[10] and Taatjes *et al.*[11] but in contrast to recommendations for atmospheric modelling based on indirect measurements. Rate coefficients for reactions of CH_2OO with NO_2 and SO_2 are essentially independent of pressure over the pressure ranges studied in this work. The rate coefficient for CH_2OO + CH_3CHO is pressure dependent, with stabilisation to form the secondary ozonide reaction products at high pressures.

We observe no evidence for reactions of CH_2OO with NO or H_2O under the conditions employed in this work, and place upper limits on rate coefficients for these reactions of 2 × 10^{-13} cm^3 s^{-1} and 9 × 10^{-17} cm^3 s^{-1}, respectively. The upper limit for the rate coefficient for CH_2OO + H_2O is significantly lower than has been reported previously. Earlier assessments[2,14,15,17] of the impacts of increased reaction rates for CH_2OO + SO_2 and CH_2OO + NO_2 will therefore be lower limits owing to over-estimation of the impacts of CH_2OO + H_2O.

Acknowledgements

The authors are grateful to the National Centre for Atmospheric Science (NCAS) and the Engineering and Physical Sciences Research Council (EPSRC, grant reference EP/J010871/1) for funding.

References

1 D. Johnson and G. Marston, *Chem. Soc. Rev.*, 2008, **37**, 699–716.
2 C. A. Taatjes, D. E. Shallcross and C. Percival, *Phys. Chem. Chem. Phys.*, 2013, DOI: 10.1039/C3CP52842A.
3 N. M. Donahue, G. T. Drozd, S. A. Epstein, A. A. Presto and J. H. Kroll, *Phys. Chem. Chem. Phys.*, 2011, **13**, 10848–10857.
4 M. S. Alam, M. Camredon, A. R. Rickard, T. Carr, K. P. Wyche, K. E. Hornsby, P. S. Monks and W. J. Bloss, *Phys. Chem. Chem. Phys.*, 2011, **12**, 11002–11015.
5 L. Vereecken, *Science*, 2013, **340**, 154–155.
6 T. L. Malkin, A. Goddard, D. E. Heard and P. W. Seakins, *Atmos. Chem. Phys.*, 2010, **10**, 1441–1459.
7 D. E. Heard, L. J. Carpenter, D. J. Creasey, J. R. Hopkins, J. D. Lee, A. C. Lewis, M. J. Pilling, P. W. Seakins, N. Carslaw and K. M. Emmerson, *Geophys. Res. Lett.*, 2004, **31**, L18112.
8 R. M. Harrison, J. Yin, R. M. Tilling, X. Cai, P. W. Seakins, J. R. Hopkins, D. L. Lansley, A. C. Lewis, M. C. Hunter, D. E. Heard, L. J. Carpenter, D. J. Creasey, J. D. Lee, M. J. Pilling, N. Carslaw, K. M. Emmerson, A. Redington,

Open Access Article. Published on 20 November 2013. Downloaded on 10/16/2025 12:40:07 PM.
This article is licensed under a Creative Commons Attribution 3.0 Unported Licence.

R. G. Derwent, D. Ryall, G. Mills and S. A. Penkett, *Sci. Total Environ.*, 2006, **360**, 5–25.
9 D. Stone, L. K. Whalley and D. E. Heard, *Chem. Soc. Rev.*, 2012, **41**, 6348–6404.
10 O. Welz, J. D. Savee, D. L. Osborn, S. S. Vasu, C. J. Percival, D. E. Shallcross and C. A. Taatjes, *Science*, 2012, **335**, 204–207.
11 C. A. Taatjes, O. Welz, A. J. Eskola, J. D. Savee, D. L. Osborn, E. P. F. Lee, J. M. Dyke, D. W. K. Mok, D. E. Shallcross and C. J. Percival, *Phys. Chem. Chem. Phys.*, 2012, **14**, 10391–10400.
12 C. A. Taatjes, O. Welz, A. J. Eskola, J. D. Savee, A. M. Scheer, D. E. Shallcross, B. Rotavera, E. P. F. Lee, J. M. Dyke, D. K. W. Mok, D. L. Osborn and C. J. Percival, *Science*, 2013, **340**, 177–180.
13 L. Vereecken, H. Harder and A. Novelli, *Phys. Chem. Chem. Phys.*, 2012, **14**, 14682–14695.
14 M. Boy, D. Mogensen, S. Smolander, L. Zhou, T. Nieminen, P. Paasonen, C. Plass-Duelmer, M. Sipila, T. Petaja, L. Mauldin, H. Berresheim and M. Kulmala, *Atmos. Chem. Phys.*, 2013, **13**, 3865–3879.
15 J. R. Pierce, M. J. Evans, C. E. Scott, S. D. D'Andrea, D. K. Farmer, E. Swietlicki and D. V. Spracklen, *Atmos. Chem. Phys.*, 2013, **13**, 3163–3176.
16 G. Sarwar, K. Fahey, R. Kwok, R. C. Gilliam, S. J. Roselle, R. Mathur, J. Xue, J. Yu and W. P. L. Carter, *Atmos. Environ.*, 2013, **68**, 186–197.
17 C. J. Percival, O. Welz, A. J. Eskola, J. D. Savee, D. L. Osborn, D. O. Topping, D. Lowe, S. R. Utembe, A. Bacak, G. McFiggans, M. C. Cooke, P. Xiao, A. T. Archibald, M. E. Jenkin, R. G. Derwent, I. Riipinen, D. W. K. Mok, E. P. F. Lee, J. M. Dyke, C. A. Taatjes and D. E. Shallcross, *Faraday Discuss.*, 2013, DOI: 10.1039/C3FD00048F.
18 C. A. Taatjes, G. Meloni, T. M. Selby, A. J. Trevitt, D. L. Osborn, C. J. Percival and D. E. Shallcross, *J. Am. Chem. Soc.*, 2008, **130**, 11883–11885.
19 Y.-T. Su, Y.-H. Huang, H. A. Witek and Y.-P. Lee, *Science*, 2013, **340**, 174–176.
20 J. M. Beames, F. Liu, L. Lu and M. I. Lester, *J. Am. Chem. Soc.*, 2012, **134**, 20045–20048.
21 B. Ouyang, M. W. McLeod, R. L. Jones and W. J. Bloss, *Phys. Chem. Chem. Phys.*, 2013, **15**, 17070–17075.
22 A. Jalan, J. W. Allen and W. H. Green, *Phys. Chem. Chem. Phys.*, 2013, **15**, 16841–16852.
23 R. L. Mauldin, III, T. Berndt, M. Sipilae, P. Paasonen, T. Petaja, S. Kim, T. Kurten, F. Stratmann, V. M. Kerminen and M. Kulmala, *Nature*, 2012, **488**, 193–197.
24 T. Kurten, J. R. Lane, S. Jorgensen and H. G. Kjaergaard, *J. Phys. Chem. A*, 2011, **115**, 8669–8681.
25 H. Huang, A. J. Eskola and C. A. Taatjes, *J. Phys. Chem. Lett.*, 2012, **3**, 3399–3403.
26 D. Stone, M. Blitz, L. Daubney, T. Ingham and P. Seakins, *Phys. Chem. Chem. Phys.*, 2013, **15**, 19119–19124.
27 H. Huang, B. Rotavera, A. J. Eskola and C. A. Taatjes, *J. Phys. Chem. Lett.*, 2013, **4**, 3824.
28 C. M. Roehl, J. B. Burkholder, G. K. Moortgat, A. R. Ravishankara and P. Crutzen, *J. Geophys. Res.: Atmos.*, 1997, **102**, 12819–12829.
29 L. J. Carpenter, W. T. Sturges, S. A. Penkett, P. S. Liss, B. Alicke, K. Hebestreit and U. Platt, *J. Geophys. Res., [Atmos.]*, 1999, **104**, 1679–1689.
30 L. J. Carpenter, *Chem. Rev.*, 2003, **103**, 4953–4962.
31 L. J. Carpenter, S. D. Archer and R. Beale, *Chem. Soc. Rev.*, 2012, **41**, 6473–6506.
32 T. J. Gravestock, M. A. Blitz, W. J. Bloss and D. E. Heard, *ChemPhysChem*, 2010, **11**, 3928–3941.
33 R. A. Cox, *J. Phys. Chem.*, 1972, **76**, 814–820.
34 J. L. Jourdain, G. Lebras and J. Combourieu, *Int. J. Chem. Kinet.*, 1979, **11**, 569–577.
35 K. J. Hughes, M. A. Blitz, M. J. Pilling and S. H. Robertson, *Proc. Combust. Inst.*, 2002, **29**, 2431–2437.
36 D. T. Co, T. F. Hanisco, J. G. Anderson and F. N. Keutsch, *J. Phys. Chem. A*, 2005, **109**, 10675–10682.
37 M. A. Blitz, A. Goddard, T. Ingham and M. J. Pilling, *Rev. Sci. Instrum.*, 2007, **78**, 034103.
38 M. Teresa Baeza-Romero, M. A. Blitz, A. Goddard and P. W. Seakins, *Int. J. Chem. Kinet.*, 2012, **44**, 532–545.
39 G. Hancock and V. Haverd, *Chem. Phys. Lett.*, 2003, **372**, 288–294.
40 H. M. Su, W. T. Mao and F. N. Kong, *Chem. Phys. Lett.*, 2000, **322**, 21–26.
41 U. Bley, F. Temps, H. G. Wagner and M. Wolf, *Ber. Bunsen-Ges. Phys. Chem.*, 1992, **96**, 1043–1048.
42 R. A. Alvarez and C. B. Moore, *J. Phys. Chem.*, 1994, **98**, 174–183.
43 M. A. Blitz, C. Kappler, M. J. Pilling and P. W. Seakins, *Z. Phys. Chem.*, 2011, **225**, 957–967.
44 A. J. Eskola, D. Wojcik-Pastuszka, E. Ratajczak and R. S. Timonen, *J. Phys. Chem. A*, 2006, **110**, 12177–12183.
45 A. J. Eskola, D. Wojcik-Pastuszka, E. Ratajczak and R. S. Timonen, *Phys. Chem. Chem. Phys.*, 2006, **8**, 1416–1424.
46 A. Masaki, S. Tsunashima and N. Washida, *J. Phys. Chem.*, 1995, **99**, 13126–13131.
47 J. C. Ianni, *Kintecus, Windows Version 2.80*, www.kintecus.com, 2002.
48 P. D. Lightfoot, R. A. Cox, J. N. Crowley, M. Destriau, G. D. Hayman, M. E. Jenkin, G. K. Moortgat and F. Zabel, *Atmos. Environ., Part A*, 1992, **26**, 1805–1961.
49 R. Atkinson, D. L. Baulch, R. A. Cox, J. N. Crowley, R. F. Hampson, R. G. Hynes, M. E. Jenkin, M. J. Rossi and J. Troe, *Atmos. Chem. Phys.*, 2006, **6**, 3625–4055.
50 O. Horie, C. Schafer and G. K. Moortgat, *Int. J. Chem. Kinet.*, 1999, **31**, 261–269.